Effect of corrugation pitch on thermo-hydraulic performance of nanofluids in corrugated tubes of heat exchanger system based on exergy efficiency

Guiqing Wang [a], Cong Qi [a, b*], Maoni Liu [a], Chunyang Li [a], Yuying Yan [b], Lin Liang [a]

[a] School of Electrical and Power Engineering, China University of Mining and Technology, Xuzhou 221116, China

[b] Fluids & Thermal Engineering Research Group, Faculty of Engineering, University of Nottingham, Nottingham NG7 2RD, UK

Abstract: In this article, water and TiO_2-H_2O nanofluids are used as heat exchange mediums. The heat transfer and resistance coefficient of corrugated tubes with different corrugation pitches are studied by experimental method. The economy of experimental system is evaluated from the aspects of quantity and quality of energy by thermal and exergy efficiencies respectively. The heat transfer performance of nanofluids in the smooth tube can be enhanced by 2.64-16.9% compared with water under the same working conditions, while the corrugated tubes can improve the heat transfer performance by 4.8-66.3%. When the mass fraction of the nanofluid is 0.5%, the corrugated tubes with different corrugation pitches can increase the heat transfer by 36.3% (*P*=6mm), 40.3% (*P*=4mm) and 44.5% (*P*=2mm) respectively. For thermal efficiency, the results prove that when the Reynolds number is larger than 6000, the comprehensive evaluation indexes of corrugated tubes are much larger than that of smooth tube, and the maximum can reach 1.5637. For exergy efficiency, the research results show that the exergy efficiency of the smooth tube is better than that of the corrugated tubes.

Keywords: Nanofluids; Forced convection; Corrugated tube; Exergy efficiency

[*] Correspondence author.
E-mail: gqwang@cumt.edu.cn (G. Wang), qicong@cumt.edu.cn (C. Qi), liumaoni@cumt.edu.cn (M. Liu), lichunyang@cumt.edu.cn (C. Li), yuying.yan@nottingham.ac.uk (Y. Yan), lianglin@cumt.edu.cn (L. Liang)

Nomenclature

A	cross-sectional area, m^2
b_i	intercept of straight line
c_1, c_2	coefficient in equation
c_p	heat capacity of nanofluids, $J\cdot kg^{-1}\cdot K^{-1}$
c_{pb}	heat capacity of base fluid, $J\cdot kg^{-1}\cdot K^{-1}$
c_{pp}	heat capacity of nanoparticles, $J\cdot kg^{-1}\cdot K^{-1}$
$C_{Q,P}$	the ratio of heat transfer rate between enhanced and reference surfaces under identical pumping power
$C_{Q,V}$	the ratio of heat transfer rate between enhanced and reference surfaces over the ratio of friction factor between enhanced and reference surfaces under identical flow rate
$C_{Q,\triangle p}$	the ratio of heat transfer rate between enhanced and reference surfaces under identical pressure drop
d_1	outer diameter of tube, m
d_2	equivalent diameter of tube, m
d_3	inner diameter of tube, m
f	frictional resistance coefficient
h	convective heat transfer coefficient, $W\cdot m^{-2}\cdot K^{-1}$
k	thermal conductivity of nanofluids, $W\cdot m^{-1}\cdot K^{-1}$
k_i	slope of straight line
L	length of tube, m
Nu	Nusselt number
p	pressure, Pa
P	pitch of corrugated tube, m
$\Delta p/\Delta L$	pressure drop per unit length, $Pa\cdot m^{-1}$
Q	heat absorbed by nanofluids, J
q_m	mass flow rate, $kg\cdot s^{-1}$
r	outside-radius of tube, m
r'	inner-radius of tube, m
Re	Reynolds number
T_{out}	outlet temperature of tube, K
T_{in}	inlet temperature of tube, K
T_f	average temperature of nanofluids, K
T_w^*	outside surface temperature of tube, K
T_w	inside surface temperature of tube, K
u	velocity of nanofluids, $m\cdot s^{-1}$

Greek symbols

δ	thickness of tube,m
η	relative heat transfer enhancement ratios
λ	thermal conductivity of tube, $W\cdot m^{-1}\cdot K^{-1}$
μ	dynamic viscosity, Pa•s
ξ	comprehensive performance index
ρ	density of fluid, $kg\cdot m^{-3}$
ρ_p	density of nanofluids, $kg\cdot m^{-3}$
ρ_{pb}	density of base fluid, $kg\cdot m^{-3}$
ρ_{pp}	density of nanoparticle, $kg\cdot m^{-3}$
φ	volume fraction,%
ω	mass fraction,%

Subscripts

m_1, m_2	exponent in equation
in	import
out	outport
0	circular tube
e	enhanced tube
p	nanofluids
pb	base fluid
pp	nanoparticle
P	under the same pumping power
Re	under the same Reynolds number
V	under the same mass flow rate
Δp	under the same pressure drop
w	wall

1 Introduction

In order to optimize the heat transfer efficiency of the heat exchanger, the investigations mainly focus on two aspects. One is to heighten the thermal conductivity of fluid and another is to optimize the surface of heat exchanger.

In the aspect of improving the thermal conductivity of fluids, nanofluids, as a new kind working fluid, have been studied by many scholars and applied in many industries, such as natural convection heat transfer [1, 2], forced convection heat transfer [3, 4], solar absorption [5, 6], clean water [7], sunlight harvest and energy storage [8], photo-thermal conversion [9, 10], CPU cooling [11, 12] and so on.

Li et al. [13] researched the thermophysical parameters of ZnO/EG nanofluids. The results demonstrated that the thermal conductivity and viscosity of the nanofluids increase with the concentration. In addition, it was proved that nanofluids exhibit Newtonian behavior when the mass fraction of nanoparticle is less than 10.5%. Ranjbarzadeh et al. [14] formulated the stable SiO_2-water nanofluids and studied their thermal properties, the results proved that the thermal conductivity of 3% SiO_2-H_2O nanofluids is enhanced by 38.2%. According to the numerical simulation study of Alnaqi et al. [15], it could be found that 6% concentration of Al_2O_3-water nanofluids can increase the Nusselt number by 5.9%. In addition, many scholars have researched the thermophysical parameters of oil-based nanofluids. Asadi et al. investigated the thermal properties of different oil-based nanofluids, including ZnO engine oil nanofluids and MgO engine oil nanofluids [16], Al_2O_3-MWCNT thermal oil hybrid nanofluids [17], $Mg(OH)_2$/MWCNT-engine oil hybrid nano-lubricant [18], MWCNT/MgO-SAE50 hybrid nano-lubricant [19]. Results showed that oil-based nanofluids exhibit Newtonian behavior at a certain temperature and the thermal conductivity and viscosity all show an increase to varying degrees. Esfe et al. used the artificial neural network to reckon and optimize the viscosity of MWCNTs-ZnO/ 5W50 nanolubricant [20] and MWCNT-Al_2O_3/5W50 nanofluids [21], which saves the cost of experimentally measuring viscosity. Asadi et al. researched the thermal conductivity of MgO-MWCNT/thermal oil hybrid nanofluids [22] and the dynamic viscosity of MWCNT/ZnO-engine oil hybrid nanofluids [23]. Results proved that the thermal conductivity of MgO-MWCNT/ thermal oil hybrid nanofluids is improved by 65%. The dynamic viscosity of MWCNT/ZnO-engine oil hybrid nanofluids decreases with the increase of temperature, and it can be reduced by up to 85% in the experimental temperature range. Sheikholeslami et al. [24] researched the effect of thermal radiation on nanofluids and the results showed that the thermal boundary layer decreases with thermal radiation. They [25] also used numerical simulation to study the effect of Hartmann numbers on heat transfer. It was found that the temperature gradient becomes smaller as the increasing Hartmann number. Afrand et al. researched the physical properties of different nanofluids. Research content includes whether the nanofluids are Newtonian fluid [26], the changes of viscosity [27] and thermal conductivity [28] with temperature. Finally, the corresponding mathematical models are proposed. Qi et al. [29] researched the heat transfer of TiO_2-H_2O nanofluids in a triangular tube and summarized that *Nu* can be improved by 52.5% when nanoparticle mass fraction is 5%. Hu et al. [30] also applied nanofluids in boiling heat transfer and obtained the similar results. When the mass fraction of graphene nanosheets nanofluids is greater than 0.02%, the critical heat flux remains unchanged essentially. Qi et al. [31] researched the influence of different nanoparticle radius on heat transfer properties using the LBM method. It was found that the small particle size has the positive effect on heat transfer. They also [32] researched the heat transfer performance of Al_2O_3 nanofluids with different base fluids by numerical simulation. The results showed that Al_2O_3-Ga and Al_2O_3-H_2O nanofluids can improve heat transfer by 86.0% and 24.5%. Allouhi et al. [33] researched the effects of various nanofluids on parabolic trough collectors. The results indicated that CuO nanofluids can improve the exergy efficiency by 9.05%. Imani-Mofrad et al. [34] researched the application of nanofluids on cooling towers. It could be found that compared with water, the graphene/water nanofluids can enhance the cooling tower characteristics by 36%, while the alumina/water nanofluids weaken the cooling tower characteristics by 14.7%. Loni et al. [35] researched the application of carbon nanotube/oil nanofluids in solar energy systems. It was found that carbon nanotube/oil nanofluids can reduce the heat loss of the experimental system and enhance the thermal efficiency. Asadi [36] researched the heat transfer performance of MWCNT-ZnO nanofluids in microchannels. Results indicated that MWCNT-ZnO nanofluids can increase the heat transfer coefficient by 42%. Rostami et al. [37] used CuO nanofluids as a coolant to study the cooling performance of PV modules. The results showed that the CuO nanofluids can reduce the surface average temperature of PV modules by 57.25% at best. Bellos et al. [38] discussed the influence of CuO nanofluids with different base fluids on heat transfer. The results indicated that oil-based nanofluids improve the thermal efficiency by 0.76% and molten salt-based nanofluids only improve it by 0.26%. Sadeghinezhad et al. [39] researched the heat transfer of graphene nanoplatelets (GNP) nanofluids in heat pipes, and investigated the influence of heat pipe tilt angle on heat transfer. Results showed that the heat transfer can be enhanced by 28.3% when the tilt angle is 60°. Mehrali et al. experimentally researched the heat transfer of graphene nanosheet (GNP) nanofluids in a laminar flow [40] and turbulent flow [41]. Results proved that GNP nanofluids can increase the heat transfer by 15% and 200% under laminar and turbulent flow respectively. In addition, Mehrali et al. [42] studied the thermal properties and heat transfer performance of nitrogen-doped graphene (NDG) nanofluids. It was indicated that the thermal conductivity of 0.06 wt% NDG nanofluid can be increased by 36.78%.

In the aspect of improving the surface of the heat exchanger, many scholars have done lots of researches. Sundar et al. [43] researched the heat transfer and resistance coefficient of strip inserts in tubes with ND-Ni nanofluids. It was summarized that the heat transfer capacity of ND-Ni nanofluid is increased by 35.43% compared with base fluid and the strip inserts in tubes can enhance the heat transfer by 93.3%. They [44] also researched the heat transfer capacity of Fe_3O_4/water nanofluids flowing in U-bend heat exchangers with inserted coils. Results demonstrated that the heat transfer can be heightened by 32.03% while the friction loss is also increased by 16.2% when *Re*=28954. Ranjbarzadeh et al. [45] reported the heat transfer capacity of water/graphene oxide nanofluids in a smooth copper tube. Results proved that the thermophysical parameters of nanofluids can be increased by up to 28%, and the heat transfer capacity can be increased by 40.3%. Goodarzi et al. [46] discussed the heat transfer capacity of Nitrogen-doped graphene (NDG) nanofluids in a double-tube heat exchanger and it was found that the nanofluids with mass fraction 0.06% can improve the heat transfer by 15.86% compared with water at a small expense of pump work. Ranjbarzadeh et al. [47] reported the heat transfer and resistance coefficient of water/graphene oxide nanofluids. The results proved that *Nu* of the nanofluids can be increased by 51.4% and *f* can be increased by 21% compared with water. Shahsavani et al. [48] discussed the heat transfer capacity of F-MWCNTs/EG-water nanofluids in a smooth tube. Results could be summarized that the heat transfer performance is enhanced with the increasing concentration of the nanofluids and the temperature of the experimental system. Xu et al. [49] numerically researched the flow of nanofluids in a tube filled with metal foam. Results proved that the interposition of foam metal in the tube improves the heat transfer, but the flow resistance is also increased greatly, and the increase of flow resistance is bigger than that of heat transfer. Sheikholeslami et al. [50] numerically reported the heat transfer capacity of nanofluids in a circular tube with helical twisted tape. Results proved that the heat transfer capacity is observably improved with the reduction of pitch ratio. They [51] also researched the heat transfer capacity of R600a/oil/CuO nanofluids as refrigerants by experimental method. The results showed that the performance evaluation parameter is enhanced with the increasing concentration of the nanofluids. Naphon et al. researched the effects of magnetic fields strength [52] and direction [53] on the flow of TiO_2

nanofluids in spiral coils tubes. Li et al. [54] reported the heat transfer of Al_2O_3-water nanofluids and analyzed the entropy generation. Results showed that the entropy generation decreases with height ratio and Reynolds number, but it increases with height ratio. Sheikholeslami et al [55, 56] used numerical simulation to investigate the exergy loss and the second law efficiency of nanofluids in a pipe. Conclusion was that exergy loss increase as the decreasing *Re*. Qi et al. [57] discussed the heat transfer capacity of nanofluids in elliptical tubes. Experimental results showed that nanofluids flowing in the elliptical tube with mass fraction 0.5% can enhance the heat transfer by 27.9%. Zhai et al. [58] experimentally measured the heat transfer capacity of nanofluids in spiral tubes and found that spiral tube with screw pitch s=10 cm can enhance the heat transfer efficiency by 62%. Mei et al. [59] researched the heat transfer capacity of Fe_3O_4-water nanofluids in a corrugated tube under the magnetic field. Results indicated that Fe_3O_4-water nanofluids under the magnetic field enhance the heat transfer by 17.6%. Karimi et al. [60] discussed the influence of cross-section and other factors on the efficiency of heat exchanger by numerical simulation. The results showed that *Nu* of elliptical tube is 10% higher than that of round tube, but the pressure drop is also increased by 25%. Bahiraei et al. [61] presented an analysis on the thermal characteristics of graphene nanofluids in a spiral heat exchanger and found that nanofluids increase the performance index by 142% when the Reynolds number is from 1000 to 3000. Sharshir et al. [62] and Bahiraei et al. [63] revealed the significance of nanofluids in heat transfer systems from the second law of thermodynamics.

The above scholars have made outstanding contributions in the application of nanofluids and enhanced heat transfer. However, there are few studies on the influence of the corrugation pitch of symmetrical corrugated tube on the heat transfer. In addition, the heat transfer area of corrugated tube is larger than that of the ordinary tubes. In this paper, the heat transfer and resistance coefficient of TiO_2-H_2O nanofluids in corrugated tubes with three different corrugation pitches (P=2, 4, 6mm) are studied and compared with smooth tube. This article uses two evaluation methods to analyze the overall efficiency of the system. One is the thermal efficiency (criteria comprehensive evaluation index) [64], and the other is the exergy efficiency criteria [65]. The two evaluation methods are adopted to analyze the system from the quantity and quality of energy.

2 Method

2.1 Experimental system

Compared with other nanoparticles, TiO_2 nanoparticles show excellent light stability and antibacterial effect, hence, TiO_2-H_2O nanofluids are chosen as heat exchange medium in this paper. The spherical TiO_2 nanoparticles used in this paper is provided by Nanjing Tianxing New Materials Co., Ltd., and the particle size of the nanoparticles is about 10 nm. The physical parameters of the deionized water and nanoparticles used in the experiment are shown in Table 1.

Table 1 Physical parameters of TiO_2 nanoparticle and deionized water.

Physical properties	ρ (kg·m−3)	c_p (J·kg−1·K−1)	μ (Pa s)	k (W·m−1·K−1)
deionized water [66]	997.1	4179	0.001004	0.6130
TiO_2 nanoparticles [66]	4250	686.2	—	8.9538

In this article, a two-step method is used to prepare TiO_2-H_2O nanofluids. The preparation flow chart of the nanofluids is shown in Fig. 1. Firstly, add TDL-ND1 dispersant in water, then stir and mix the mixed solution with a mechanical stirrer, add nanoparticles into the mixture, and then stir the mixed solution with a mechanical stirrer and a magnetic stirrer to make the particles fully distribute in the base liquid. Then, NaOH solution was added into the mixed solution, and after adjusting the pH value of the solution to 8, and the mixed solution is placed in an ultrasonic vibration device for ultrasonic vibration, finally, the stable TiO_2-H_2O nanofluids are obtained.

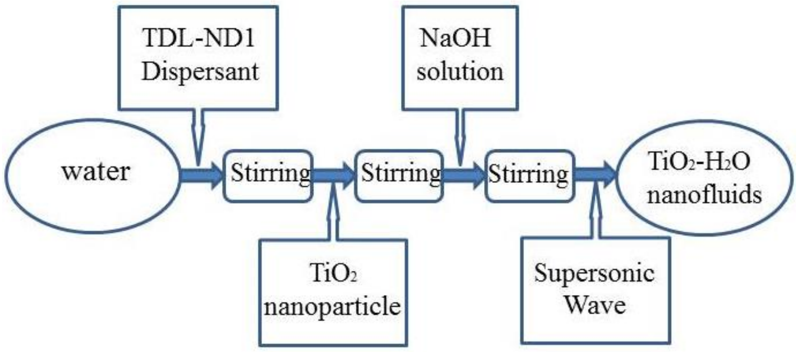

Fig. 1 Preparation of TiO_2-H_2O nanofluids

The concentration of the nanofluids in this paper is expressed by mass fraction. The mass fraction means the percentage of nanoparticles to the total weight of the nanofluids. The nanofluids with mass fractions of 0.1%, 0.3% and 0.5% are prepared in this paper. Take 1000g nanofluids as an example, the specific parameters are shown in Table 2.

Table 2 Preparation materials (Take 1000g nanofluids as an example)

Mass fraction	0.1%	0.3%	0.5%
Water/g	939	937	935
Nanoparticle/g	1	3	5
Dispersant(TDL-ND1)/g	60	60	60

Based on our previous studies [66], the authors found that nanofluids have the best stability when the concentration of the dispersant is 6% and the pH of the nanofluids is 8. Moreover, it is found that the nanofluids have no obvious precipitation after standing for 7 days, so that the prepared nanofluids are ensured to have good stability.

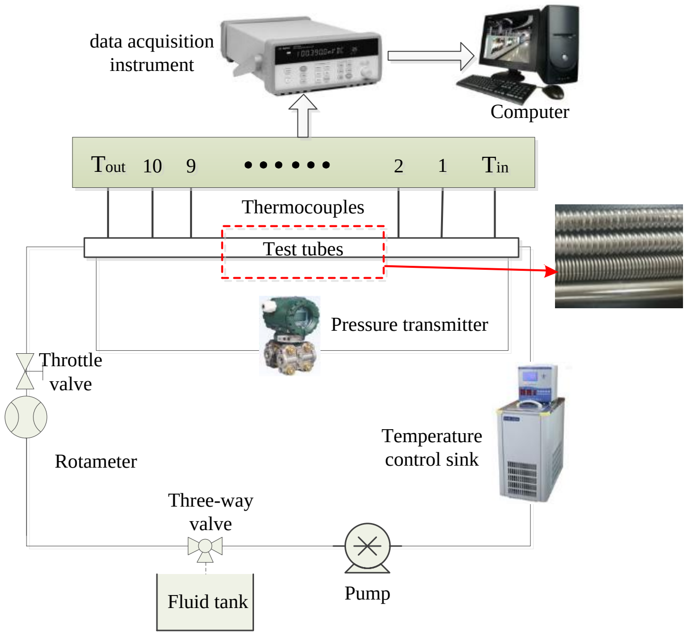

Fig. 2 Schematic diagram of the experimental system.

The schematic diagram of the experimental system in this paper is shown in Fig. 2. It can be seen that the experimental system is mainly divided into the heat transfer characteristics section and resistance test section. The heat transfer characteristics section is the core part of the experimental system which consists of a stainless steel smooth tube (corrugated tube). The parameters of the smooth tube and corrugated tubes are shown in Fig. 3 and Table 3. In order to measure the average temperature of the tube wall, ten surface mount device thermocouples are evenly distributed on the outer wall of the tube, and two armored thermocouples are arranged at the inlet and outlet of the tube to measure the temperatures of the working fluid respectively. An Agilent data acquisition instrument connected to a computer is used for collecting the temperatures. Heating wire connected with a DC power is uniformly twined on the outside of the tube to provide heat to the experimental system. For reducing heat loss, the wall is covered with insulation. The materials of the insulating layer are Aluminum silicate insulation asbestos and rubber tube sleeve. The resistance test section is also important in the experimental system. The power of the system flow is provided by a pump and the pressure drop between the inlet and outlet is tested by a pressure transmitter. 100mm of the left and right ends of the test tube are not included in the measuring section. This method is used to avoid the entrance effect on the experiment.

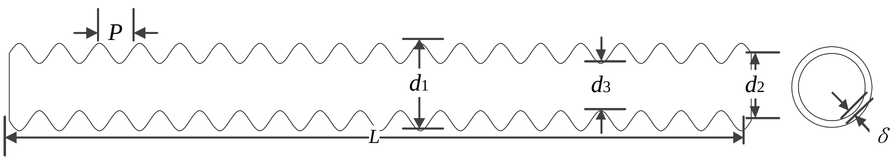

Fig. 3 Schematic diagram of the corrugated tube.

Table 3 Parameters of the tubes.

Tube specification		Geometry dimension					
		L(mm)	d_1(mm)	d_2(mm)	d_3(mm)	δ(mm)	P(mm)
Smooth tube	Tube 1	1200	-	10	-	1	-
Corrugated tube	Tube 2	1200	11.5	10	8.5	1	6
	Tube 3	1200	11.5	10	8.5	1	4
	Tube 4	1200	11.5	10	8.5	1	2

2.2 Experimental data processing

The equivalent diameter of the corrugated tube can be expressed as:

$$d_2 = \frac{4A}{L} \tag{1}$$

According to Newton’s law of cooling, the heat absorbed by the fluid is as follows:

$$Q = c_p q_m \left(T_{out} - T_{in}\right) \tag{2}$$

The formula for the convection heat transfer coefficient is calculated as follows:

$$h = \frac{Q}{\pi d_2 L(T_w - T_f)} \tag{3}$$

where T_f is the average temperature of the fluid, the formula is as follows:

$$T_f = \frac{(T_{out} + T_{in})}{2} \tag{4}$$

According to Fourier's law of heat conduction, the formula of T_w is as follows:

$$T_w = T_w^* - \frac{Q \ln(r/r')}{2\pi\lambda L} \tag{5}$$

where the formula of T_w^* is as follows:

$$T_w^* = \frac{(T_1 + T_2 + \cdots + T_{10})}{10} \tag{6}$$

The formula of Nusselt number is as follows:

$$Nu = \frac{hd_2}{k} \tag{7}$$

According to law of Darcy-Weisbach, the formula of resistance coefficient is as follows:

$$f = \frac{2d_2}{\rho u^2} \cdot \frac{\Delta p}{\Delta L} \tag{8}$$

The formula of Reynolds number is as follows:

$$Re = \rho ud / \mu \tag{9}$$

Based on our previous research [65], the density and specific heat of the nanofluids are calculated by Eqs. (10) and (11) respectively:

$$c_p = (1-\varphi)c_{pb} + \varphi c_{pp} \tag{10}$$

$$\rho_p = (1-\varphi)\rho_{pb} + \varphi\rho_{pp} \tag{11}$$

3 Results and discussions

3.1 Experimental system validation

In order to test the reliability and accuracy of the experimental system, this part compares the heat transfer and resistance coefficient of water in a smooth tube with published literature results [67] and empirical formulas [68]. The results of the comparison are shown in Fig. 4. It can be proved from the figure that the experimental results in this paper are highly consistent with the published results and the maximum error is less than 6%. Therefore, it can be seen that the reliability of the experimental platform is guaranteed.

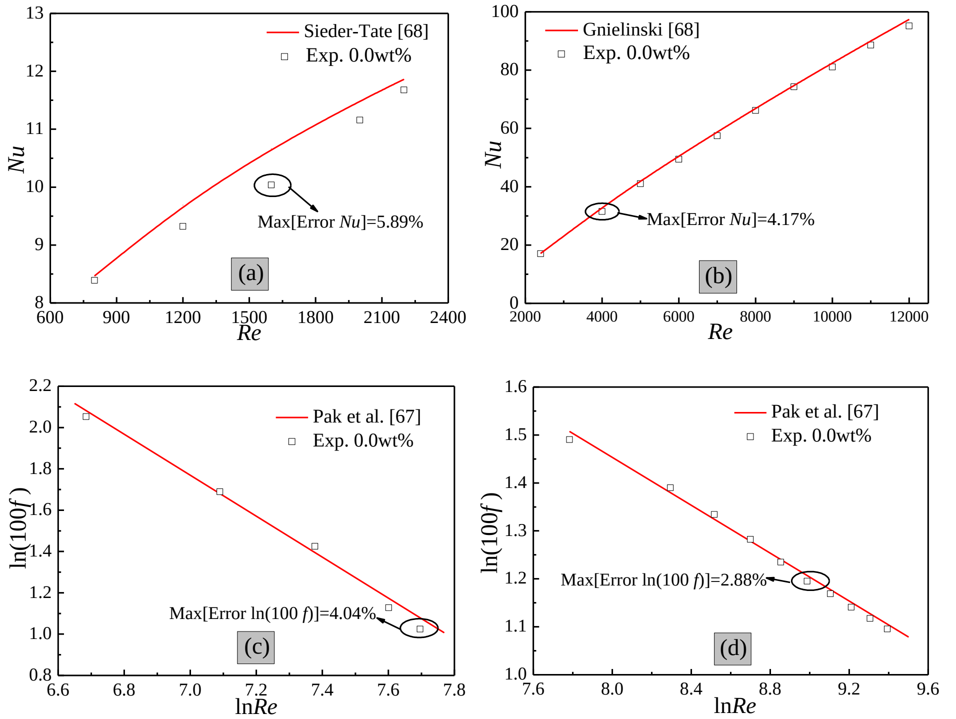

Fig. 4 Heat transfer and flow characteristics of deionized water in a smooth tube. (a) *Nu*-laminar flow, (b) *Nu*-turbulent flow, (c) *f*-laminar flow, (d) *f*-turbulent flow.

3.2 Uncertainty analysis

In this paper, the uncertainty of the experiment is calculated to ensure the accuracy of the experiment. *Nu* and *f* are the main features in this study. The formulas are as follows:

$$\frac{\delta Nu}{Nu} = \sqrt{(\frac{\delta Q}{Q})^2 + (\frac{\delta T}{T})^2} \tag{12}$$

$$\frac{\delta f}{f} = \sqrt{(\frac{\delta p}{p})^2 + (\frac{\delta L}{L})^2 + (\frac{\delta q_m}{q_m})^2} \tag{13}$$

The uncertainty of the experiment is due to instrument errors and measurement errors. The latter can be avoided through multiple experiments, but the former cannot be avoided. The uncertainties of the instruments used in this experiment are shown in Table 4. According to the calculations of Eqs (12) and (13), The uncertainties of *Nu* and *f* are 1.41% and 1.06% respectively.

Table 4 Experimental equipment and their accuracies

Experimental equipment	DC-Power (Q)	thermocouple (T)	pressure transducer (p)	length (L)	mass flow rate (q_m)
Uncertainty	±1%	±1%	±0.5%	±0.1%	1.06%

3.3 Experimental results and discussions

3.3.1 Analysis of heat transfer performance

Fig. 5 gives the changes of the Nusselt number with the Reynolds number. The conclusion can be summarized that the heat transfer capacity of the fluid in the tube

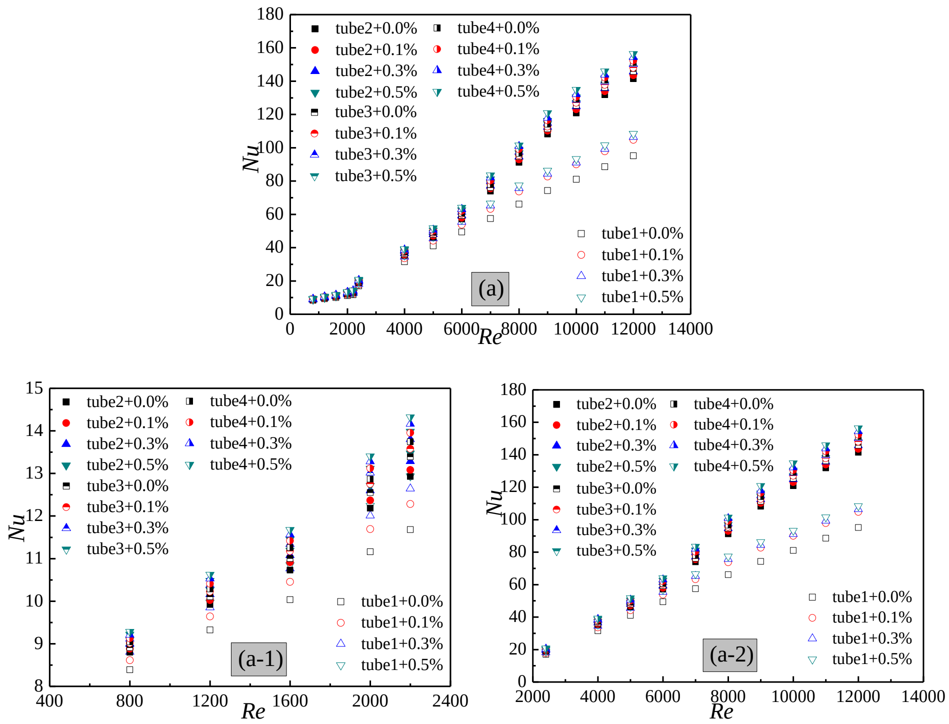

Fig. 5 Nusselt numbers of nanofluids. (a) Nusselt numbers at different Reynolds numbers, (a-1) laminar flow, (a-2) turbulent flow.

becomes better with the increase of Reynolds number. The reason may be that the increase of Reynolds number means an increase of speed, which strengthens the disturbance of the fluid, destroys the boundary layer and lastiy enhances the heat transfer.

3.3.1.1 Effect of nanoparticle mass fraction

Fig. 6 shows the effect of adding nanoparticles on the Nusselt numbers. The eight subgraphs are the heat transfer results of a smooth tube and corrugated tubes with three different corrugation pitches in laminar flow and turbulent flow. The conclusion can be summarized as that with the mass fraction of nanoparticles increases, the heat transfer performance increases. This is because the thermal conductivity of nanoparticles is obviously larger than that of the water, the addition of nanoparticles enhances the thermal conductivity of the fluid. In addition to the high thermal conductivity of the nanofluids, there is an important factor which is the existence of large Brownian force, and it is the difference between nanofluids and ordinary two-phase fluids. Because the large Brownian force can destroy the flow boundary layer, strengthen the disturbance, and then enhance the heat transfer. However, it can be obtained that the heat transfer enhancement ratio from 1% to 3% is greater than that from 3% to 5%. This is because that the addition of nanoparticles in water not only improves the thermal conductivity, but also increases the viscosity of the fluid, which is a disadvantageous for heat transfer enhancement. Therefore, it is impossible to increase the mass fraction of nanoparticles without limitation to enhance the heat transfer.

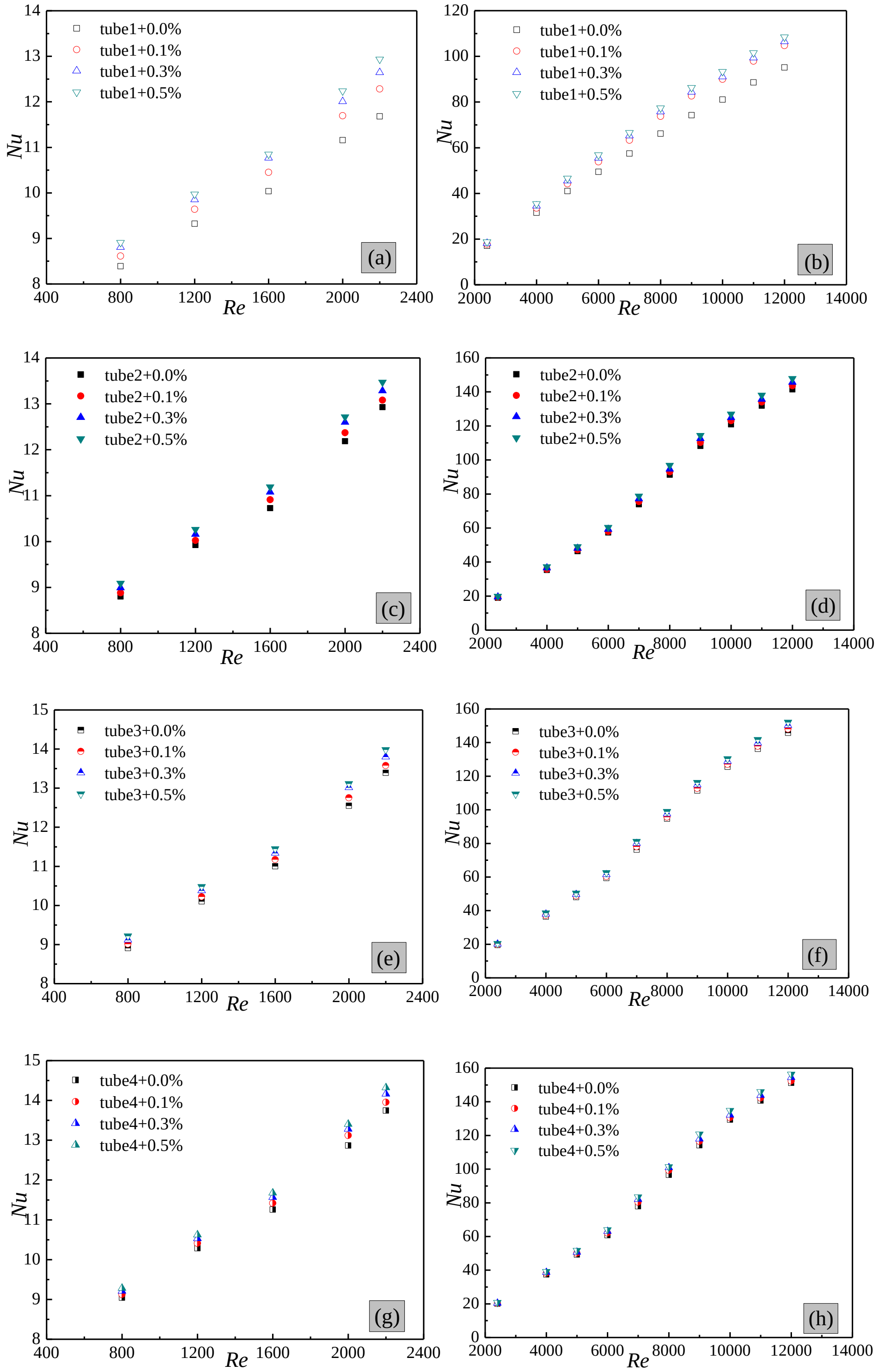

Fig. 6 Effects of nanoparticle mass fractions on Nusselt numbers of smooth tube and corrugated tube. Tube1: (a) laminar flow, (b) turbulent flow. Tube2: (c) laminar flow, (d) turbulent flow. Tube3: (e) laminar flow, (f) turbulent flow. Tube4: (g) laminar flow, (h) turbulent flow.

3.3.1.2 Effect of the structure of tube

The eight subgraphs in Fig. 7 represent the heat transfer capacity of different nanoparticle mass fractions in laminar flow and turbulent flow.

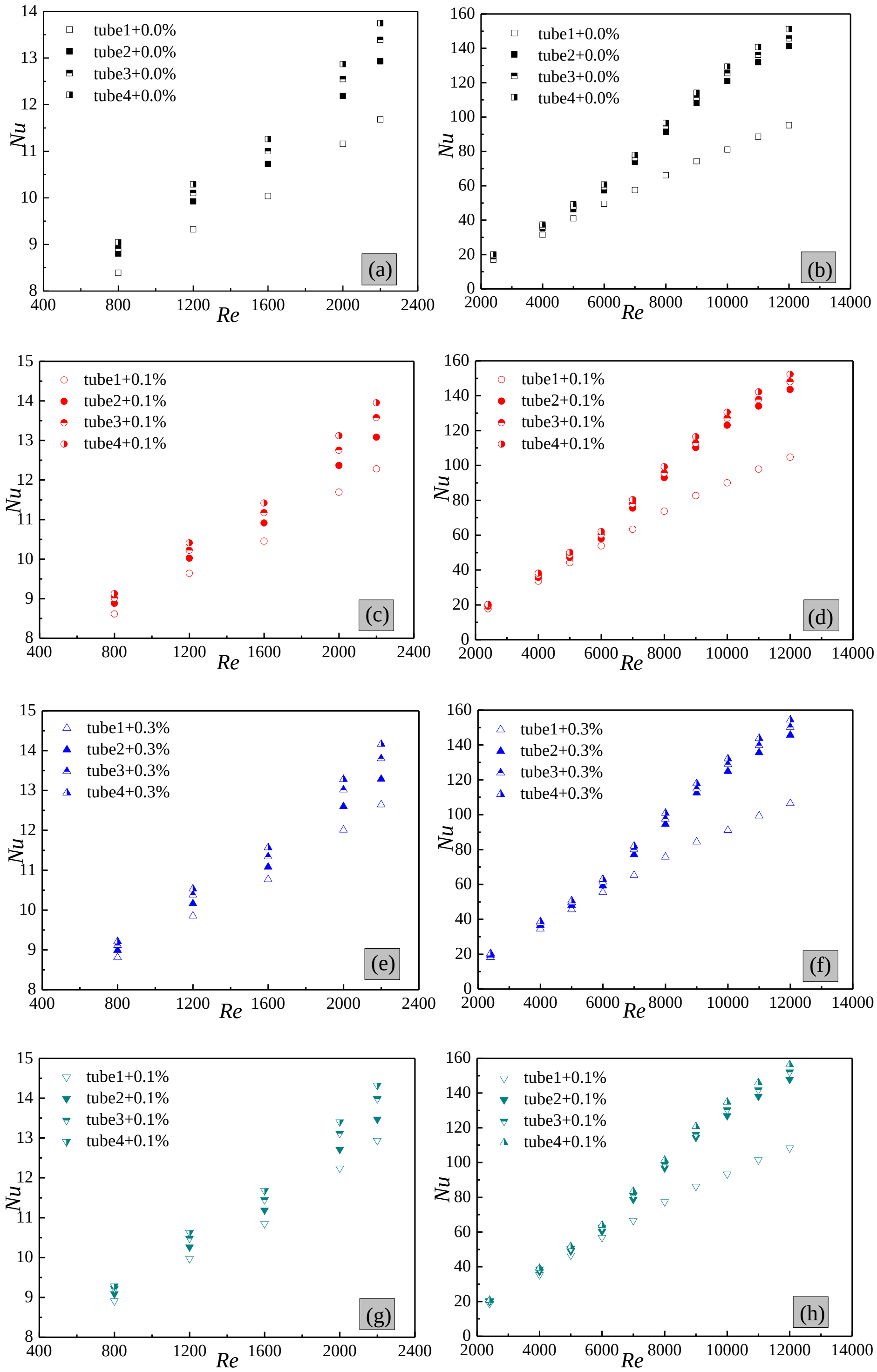

Fig. 7 Effects of tube structures on Nusselt numbers. ω=0.0%: (a) laminar flow, (b) turbulent flow. ω=0.1%: (c) laminar flow, (d) turbulent flow. ω=0.3%: (e) laminar flow, (f) turbulent flow. ω=0.5%: (g) laminar flow, (h) turbulent flow.

It can be obtained that the heat transfer performance is less influenced by the changes of the corrugation pitch when the Reynolds number is less than 6000. When the Reynolds number increases, the vortex generated is larger and the backflow is stronger, and the heat transfer capacity is more influenced by the structure of tube. Therefore, under the condition that the Reynolds number increases, the heat transfer capacity of corrugated tube is obviously stronger than that of smooth tube. The heat transfer capacity of corrugated tube with different corrugation pitches is also different. As can be seen from the various subgraphs, tube 4 has the best heat transfer performance. This is because the corrugation pitch of the corrugated tube 4 is the smallest, and a small corrugation pitch will cause the fluid to generate a more intense secondary reflux, which washes the walls and thins the boundary layer and it can cause an increase in the temperature gradient. At the same time, nanoparticles further disrupt the flow boundary layer in the secondary flow and then enhance the heat transfer.

3.3.1.3 Heat transfer enhancement ratio

In order to clearly see the effect of nanofluid and tube structures on heat transfer performance, all working conditions are compared with the flow of water in the smooth tube according to formula (14). Results are shown in Fig. 8.

$$\eta = \frac{Nu - Nu_{\text{water+circular tube}}}{Nu_{\text{water+circular tube}}} \tag{14}$$

It can be obtained that the heat transfer enhancement of corrugated tube is significantly stronger than that of smooth tube. In laminar flow, the heat transfer capacity of the nanofluids in smooth tube and corrugated tubes is enhanced by 2.64-22.62% compared with water flowing in the smooth tube. In turbulent flow, it can be enhanced by 4.3-66.34%. When the Reynolds number exceeds 6000, the heat exchange capacity of the corrugated tubes far exceeds that of smooth tube. The heat transfer capacity of nanofluids in the smooth tube can be enhanced by 2.64-16.9% under the same working conditions compared with water, while the corrugated tubes can enhance the heat transfer by 4.8-66.3%. When the mass fraction of the nanofluid is 0.5%, the corrugated tubes with different corrugation pitches can increase the heat transfer by 36.3% (P=6mm), 40.3% (P=4mm) and 44.5% (P=2mm) respectively. In addition, it can be seen from Fig. 8 that the smooth tube and corrugated tubes at Re=8000 and Re=10000 show the largest heat transfer enhancement ratio respectively. The relative heat transfer enhancement ratio (η) is basically unchanged when the Reynolds number exceeds the critical Reynolds number.

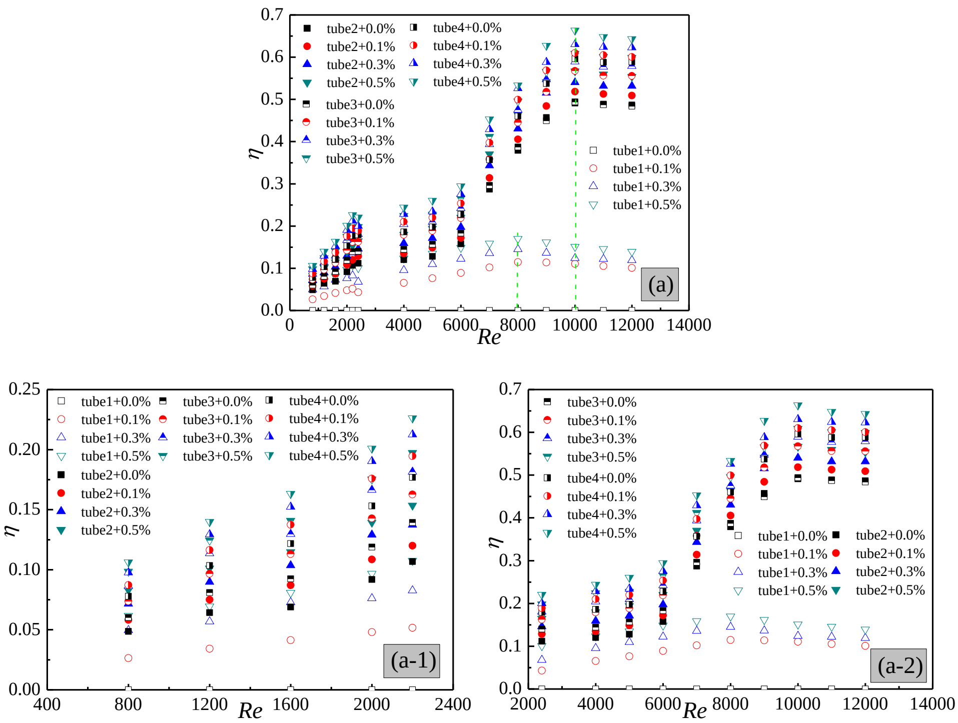

Fig. 8 Relative heat transfer enhancement ratios. (a) relative heat transfer enhancement ratios at different Reynolds numbers, (a-1) laminar flow, (a-2) turbulent flow.

3.3.2 Analysis of resistance performance

It can be concluded from the Fig. 9 that the resistance coefficient decreases as the increase of Reynolds number in laminar flow and turbulent flow respectively. This is consistent with Eq. (8). For the frictional resistance coefficients of nanofluids, there is a small increase with nanoparticle mass fractions, and the frictional resistance coefficients of nanofluids are close to each other. The reason is that the increase of frictional resistance coefficients caused by the increase of nanoparticle mass fractions is far less than the influence of different tube types. In order to clearly see the effect of nanoparticle mass fraction and tube shape on the drag coefficient, the nanoparticle mass fraction and tube type, as variables, are analyzed respectively.

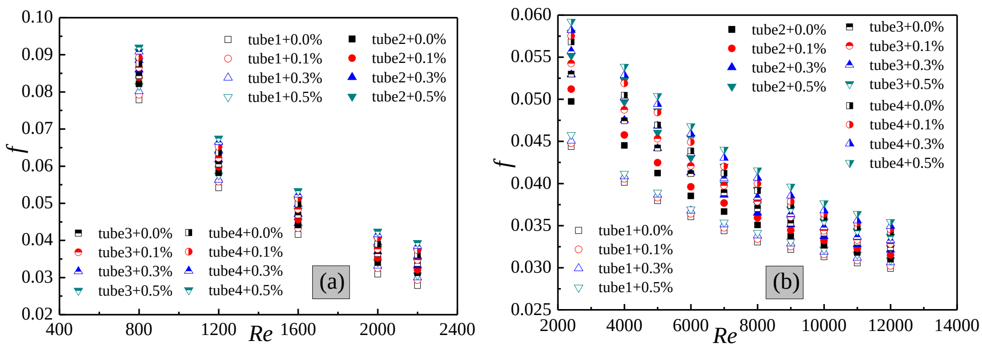

Fig. 9 Resistance coefficients of nanofluids at different Reynolds numbers. (a) laminar flow, (b) turbulent flow.

3.3.2.1 Effect of nanoparticle mass fraction

Fig. 10 shows the effect of adding nanoparticles on the resistance coefficient. The eight subgraphs are the results of a smooth tube and corrugated tubes with three different corrugation pitches in laminar flow and turbulent flow. Under the same Reynolds number, the resistance coefficient increases with the nanoparticle mass fraction. This is because the viscosity of the nanofluids increases with the increasing nanoparticles, which causes an increase in friction loss, therefore, the resistance coefficient increases.

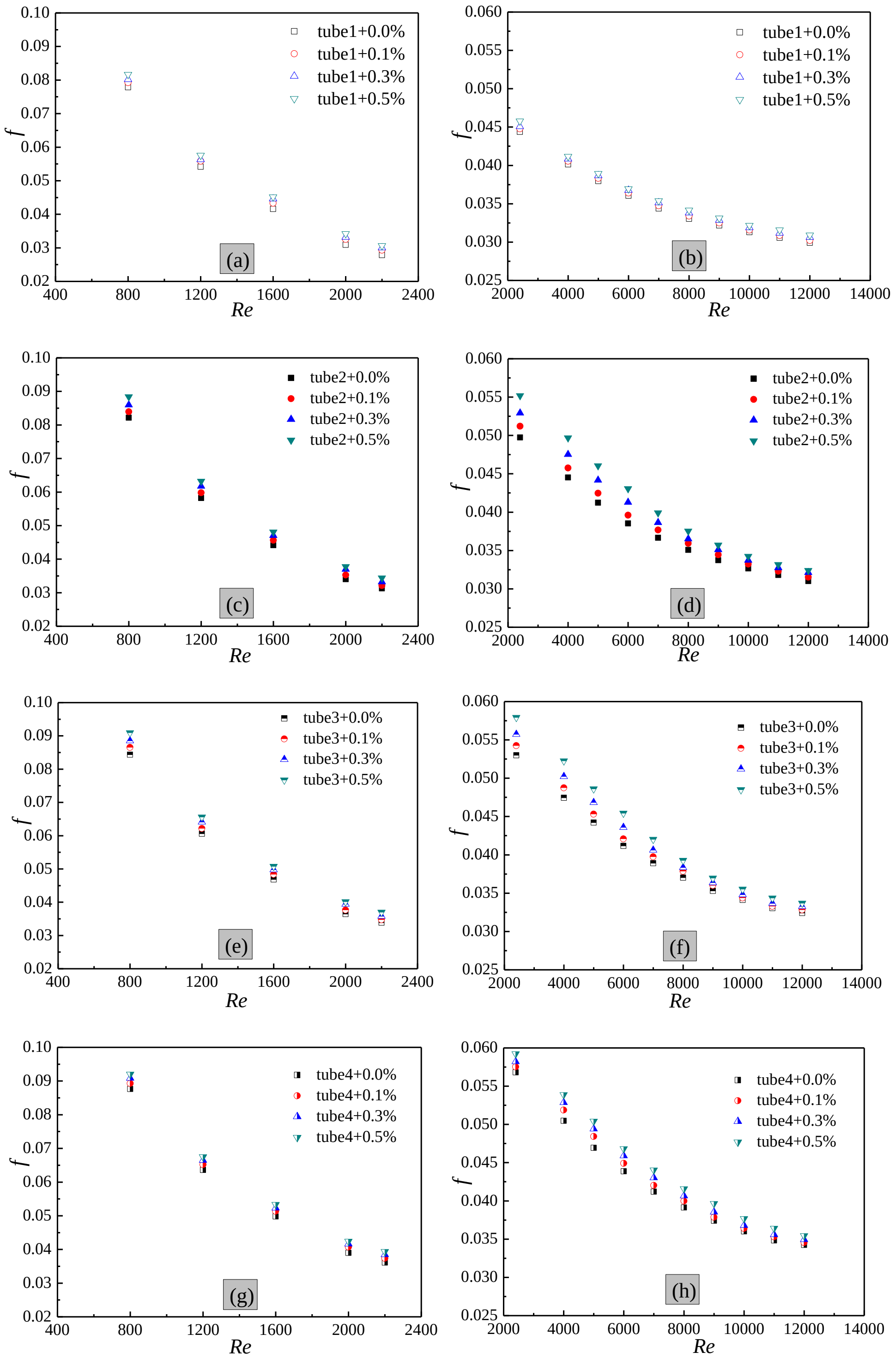

Fig. 10 Effects of nanoparticle mass fractions on resistance coefficients of smooth tube and corrugated tube. Tube1: (a) laminar flow, (b) turbulent flow. Tube2: (c) laminar flow, (d) turbulent flow. Tube3: (e) laminar flow, (f) turbulent flow. Tube4: (g) laminar flow, (h) turbulent flow.

3.3.2.2 Effect of the structure of tube

Fig. 11 gives the effect of different tube structures on the resistance coefficient under the same nanoparticle mass fraction.

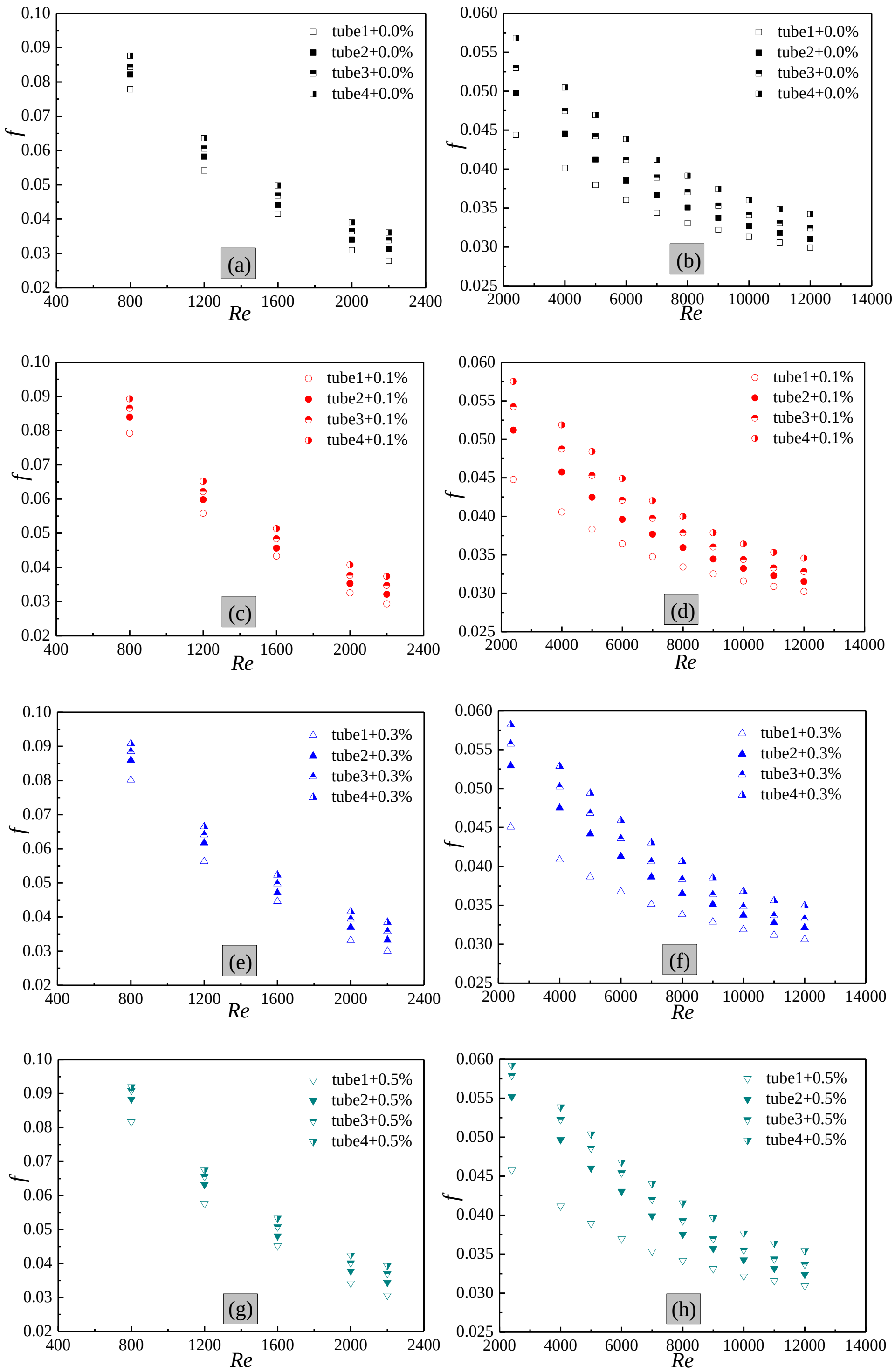

Fig. 11 Effects of tube structures on resistance coefficients. ω=0.0%: (a) laminar flow, (b) turbulent flow. ω=0.1%: (c) laminar flow, (d) turbulent flow. ω=0.3%: (e) laminar flow, (f) turbulent flow. ω=0.5%: (g) laminar flow, (h) turbulent flow.

It can be concluded that the resistance coefficients of corrugated tubes are markedly bigger than that of smooth tube. From the analysis of perspective of fluid mechanics, as the fluid flows through the trough, the static pressure decreases and the velocity increases. Conversely, as the fluid flows through the peak, the static pressure increases and the velocity decreases. Thus vortexes are generated which increases the pressure loss and resistance coefficient. When the corrugation pitch of the corrugated tube becomes small, the resistance coefficient increases, which has the similar reasons.

3.3.3 Comprehensive evaluation index

According to above researches on the heat transfer and resistance characteristics of the tubes, the combination of corrugated tube and nanofluids increases the Nusselt number to varying degrees, but the resistance coefficient also increases. Therefore, it is inaccurate to only use the improvement of Nusselt number to evaluate the system. The comprehensive performance index (thermal efficiency) is proposed to solve this problem well, and it is adopted to evaluate the heat transfer performance considering the Nusselt number and flow resistance coefficient comprehensively. It is one of the effective methods to judge the heat transfer of enhanced tubes. The evaluation criteria of the comprehensive performance index is as follows [64]:

$$\xi = \left(\frac{Nu}{Nu_{\mathrm{water+smooth}}}\right) \Bigg/ \left(\frac{f}{f_{\mathrm{water+smooth}}}\right)^{\frac{1}{3}} \tag{15}$$

Fig. 12 shows the comprehensive performance indexes. It can be seen from Fig. 12 that the trend of the comprehensive performance index is consistent with the relative heat transfer enhancement ratio, which indicates that Nusselt number dominates the comprehensive evaluation. The comprehensive evaluation indexes of corrugated tubes are obviously larger than that of smooth tube under the same Reynolds number. The maximum evaluation index of the smooth tube can reach 1.156, while the corrugated tubes can reach 1.5637. It can be seen from Fig. 12, smooth tube and corrugated tubes have different critical Reynolds numbers. The critical Reynolds number of smooth tube is 8000, but the critical Reynolds number of corrugated tube is 10000. When the Reynolds number exceeds the critical Reynolds number, the comprehensive evaluation index is basically unchanged. In addition, it can be seen that the comprehensive performance indexes of the corrugated tubes in the transition zone are basically the same as that of the smooth tube when *Re*=8000, which indicates that the corrugated tubes can obtain higher heat exchange efficiency with less pump work.

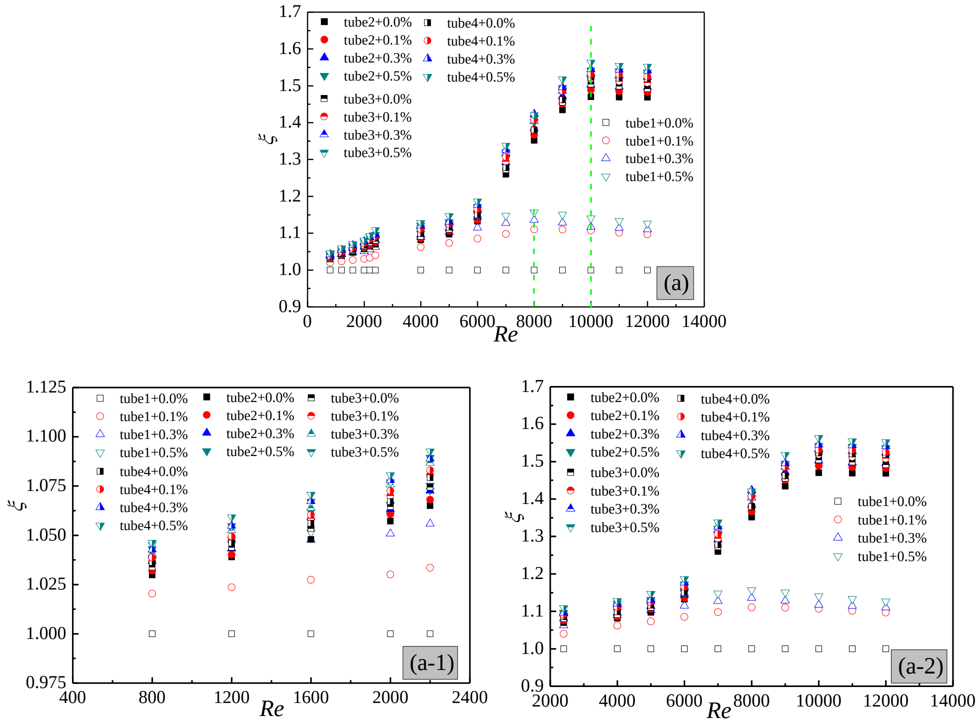

Fig. 12 Comprehensive performance indexes. (a) comprehensive performance indexes at different Reynolds numbers, (a-1) laminar flow, (a-2) turbulent flow.

3.3.4 Exergy efficiency evaluation

The comprehensive evaluation index comprehensively evaluates the economic efficiency of the system from energy consumption (resistance coefficient) and output (Nusselt number), but it does not consider the quality of energy. An exergy efficiency criterion is developed by our previous published reference [65], which is used to evaluate the change in energy quality of the fluid in the enhanced tubes.

The formula for exergy efficiency of heat exchange tubes is obtained [65]:

$$C_{Q,i} = \left(\frac{Nu_{\mathrm{e}}}{Nu_0}\right)_{Re} \Bigg/ \left(\frac{f_{\mathrm{e}}}{f_0}\right)_{Re}^{k_i} (i = P, \Delta p, V) \tag{16}$$

where $f_0(Re) = c_1 Re^{\mathrm{m}_1}$, $Nu_0(Re) = c_2 Re^{\mathrm{m}_2}$, $k_P = \frac{\mathrm{m}_2}{3+\mathrm{m}_1}$, $k_{\Delta p} = \frac{\mathrm{m}_2 - 1}{2+\mathrm{m}_1}$, $k_V = 1$.

Take the logarithm of both sides of Eq (16):

$$\ln\left(\frac{Nu_{\mathrm{e}}}{Nu_0}\right)_{Re} = b_i + k_i \ln\left(\frac{f_{\mathrm{e}}}{f_0}\right)_{Re} \tag{17}$$

where $b_P = \ln C_{Q,P}$, $b_{\Delta p} = \ln C_{Q,\Delta p}$, $b_V = \ln C_{Q,V}$, $-1 \le \mathrm{m}_1 < 0$, $0 < \mathrm{m}_2 < 1$.

According to Eq. (17), the exergy efficiency evaluation plot is shown in Fig. 13 [65].

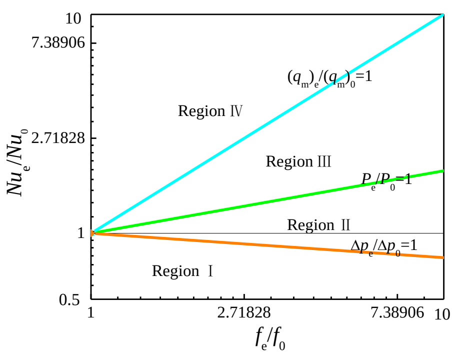

Fig. 13 Performance evaluation plot for exergy efficiency [65]

When the point is in Region Ⅳ, it means that the exergy efficiency of enhanced tube is better than that of smooth tube under all three conditions (the same mass flow, the same pump power, the same pressure drop). When the point is in Region Ⅲ, it means that the exergy efficiency of the enhanced tube is better than that of smooth tube under the same pressure drop and the same pump power, but it deteriorates under the same mass flow. When the point is in Region Ⅱ, it means that the exergy efficiency of enhanced tube is better than that of smooth tube under the same pressure drop, but it deteriorates under the same mass flow and the same pump power. When the point is in Region Ⅰ, it means that the exergy efficiency of enhanced tube is worse than that of smooth tube under all three conditions (the same mass flow, the same pump power, the same pressure drop).

Fig. 14 shows the exergy efficiency of nanofluids with different mass fractions in smooth tube and corrugated tubes. The subgraphs (a-1, b-1, c-1, d-1) represent the exergy efficiency of the four tubes, and the subgraphs (a-2, b-2, c-2, d-2) represent the slopes of the points in subgraphs (a-1, b-1, c-1, d-1). Fig. 15 shows the exergy efficiency of smooth tube and corrugated tubes under the same mass fractions of nanofluids. The subgraphs (a-1, b-1, c-1, d-1) represent the exergy efficiency of nanofluids with different mass fractions, and the subgraphs (a-2, b-2, c-2, d-2) represent the slopes of the points in subgraphs (a-1, b-1, c-1, d-1).

It can be seen that k_i decreases with the mass fraction of the nanoparticles, which indicates that the exergy efficiency decreases. The reason may be that an increase in the mass fraction of the nanofluids leads to an increase in viscosity. The viscosity of fluid means that there is internal friction when the fluid flows, and energy is consumed to overcome the internal friction, which means that the quality of the energy is reduced. It can be also found that all the points are in Region Ⅳ and

Region Ⅲ, which indicates that the exergy efficiency of the experimental system is improved compared to water flowing in the smooth tube under the same pump power.

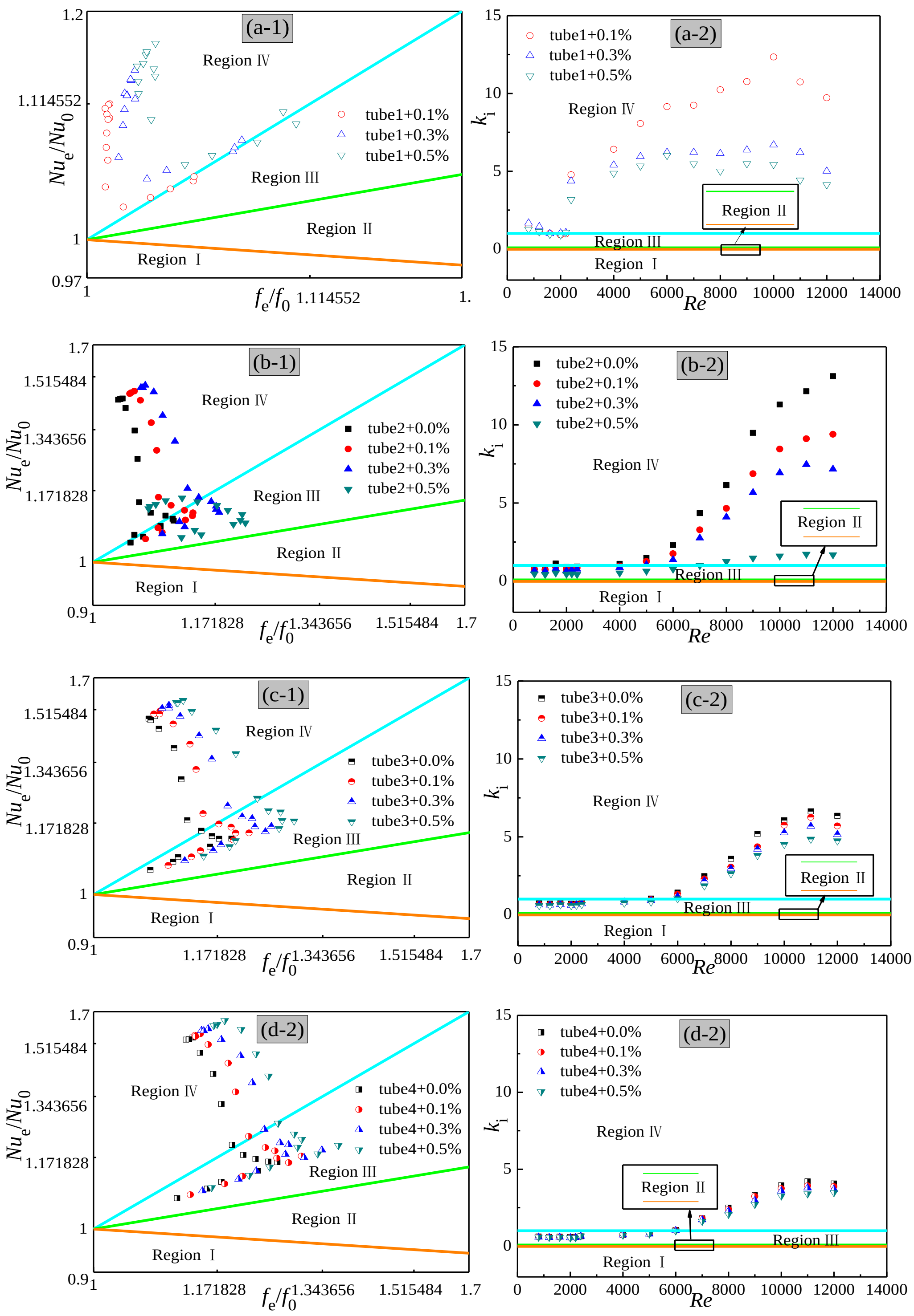

Fig. 14 Effects of nanoparticle mass fractions on exergy efficiency and slopes. Exergy efficiency: (a-1) tube1, (b-1) tube2, (c-1) tube3, (d-1) tube4. Slope: (a-2) tube1, (b-2) tube2, (c-2) tube3, (d-2) tube4.

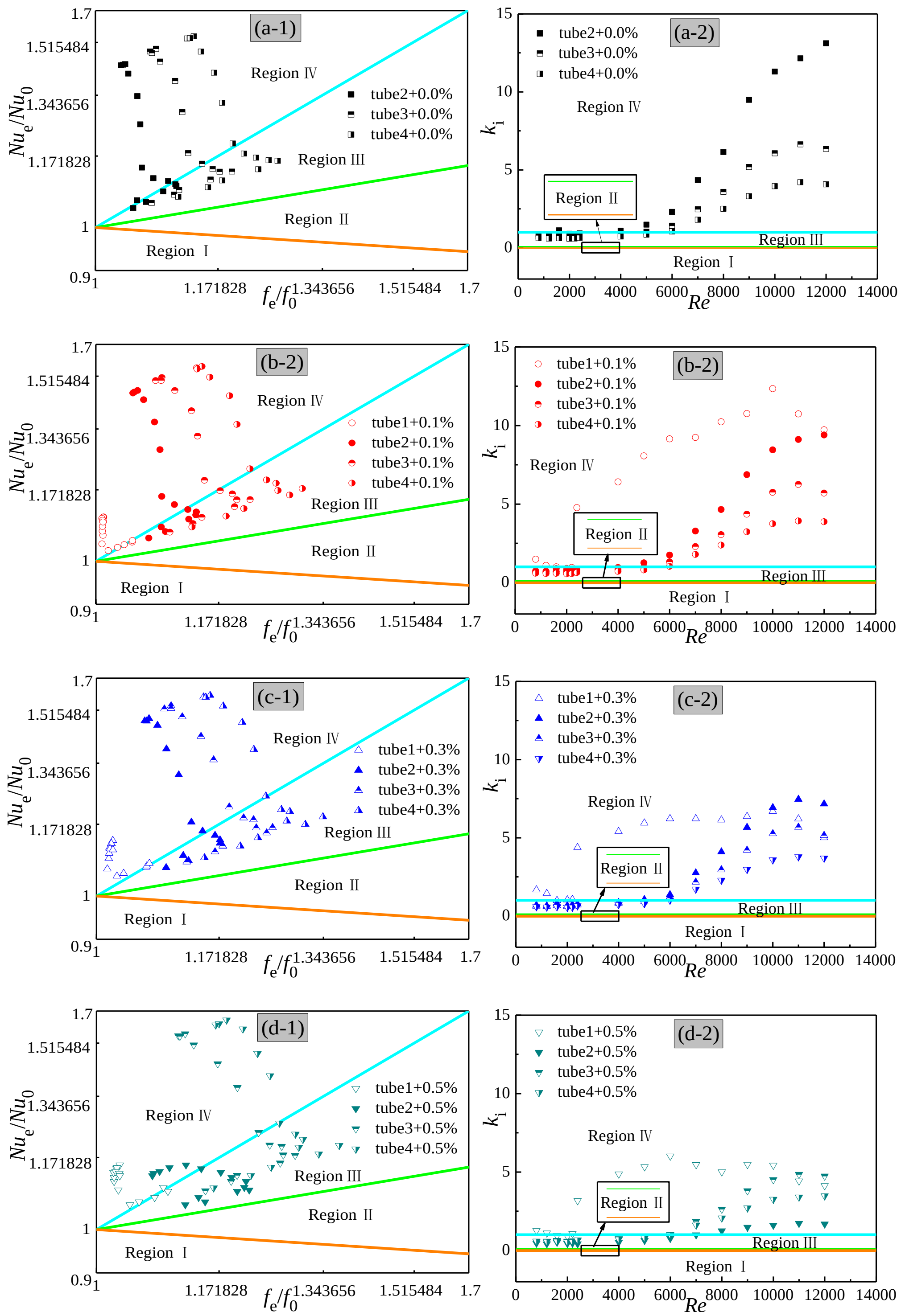

Fig. 15 Effects of tube structure on exergy efficiency and slopes. Exergy efficiency: (a-1) ω=0.0%, (b-1) ω=0.1%, (c-1) ω=0.3%, (d-1) ω=0.5%. Slope: (a-2) ω=0.0%, (b-2) ω=0.1%, (c-2) ω=0.3%, (d-2) ω=0.5%.

As can be seen from the Fig.14 and Fig.15, the exergy efficiency of the smooth tube is the best, and the exergy efficiency of the corrugated tubes decreases with the decreasing corrugation pitch. It indicates that the exergy efficiency of smooth tube is stronger than that of the corrugated tubes. This indicates that corrugated tubes make an important contribution to the reduction of energy quality. As can be seen from the subgraphs (a-2, b-2, c-2, d-2), most of the points are in Region Ⅲ in laminar flow. However, as the Reynolds number increases, the points gradually are close to Region Ⅳ. It means that the exergy efficiency is generally improved with the Reynolds number.

4 Conclusion

The heat transfer and resistance coefficient of corrugated tubes with different corrugation pitches were studied by experimental method and the experimental system was evaluated from the aspects of quantity and quality of energy by thermal and exergy efficiency respectively. The main conclusions obtained from the experiment are as follows:

(1) Compared with water, the heat transfer performance of nanofluids in smooth tube can be enhanced by 2.64-16.9% under the same working conditions, while the corrugated tubes can enhance heat transfer performance by 4.8-66.3%.

(2) Heat transfer performance increases with decreasing corrugation pitch. When the mass fraction of the nanofluid is 0.5%, the corrugated tubes with different corrugation pitches can increase the heat transfer by 36.3% (P=6mm), 40.3% (P=4mm) and 44.5% (P=2mm) respectively.

(3) Corrugated tubes and smooth tube have different critical Reynolds numbers for the maximum of comprehensive evaluation index. The smooth tube is 8000, and the corrugated tubes are 10000. The comprehensive evaluation index is basically

unchanged when the Reynolds number exceeds the critical Reynolds number.

(4) The results indicate that when the Reynolds number exceeds 6000, the comprehensive evaluation index of corrugated tubes is much larger than that of smooth tube. The maximum comprehensive evaluation index of smooth tube can reach 1.156, while the corrugated tubes can reach 1.5637.

(5) The exergy efficiency of the smooth tube is better than that of the corrugated tubes. This indicates that corrugated tubes have an important contribution to the reduction of energy quality.

Acknowledgements

This work is financially supported by "National Natural Science Foundation of China" (Grant No. 51606214), "Natural Science Foundation of Jiangsu Province, China" (Grant No. BK20181359) and "Postgraduate Research & Practice Program of Education & Teaching Reform of CUMT" (Grant No.YJSJG-2018-037).

References

[1] Sheremet MA, Pop I, Mahian O. Natural convection in an inclined cavity with time-periodic temperature boundary conditions using nanofluids: Application in solar collectors. Int J Heat Mass Transf 2018; 116: 751-761.

[2] Shi L, He Y, Hu Y, Wang X. Thermophysical properties of Fe_3O_4@CNT nanofluid and controllable heat transfer performance under magnetic field. Energy Convers Manage 2018; 177: 249-257.

[3] Mohebbi R, Rasidi MM, Izadi M, Sidik NAC, Xian HW. Forced convection of nanofluids in an extended surfaces channel using lattice Boltzmann method. Int J

Heat Mass Transf 2018; 117: 1291-1303.

[4] Sheikholeslami M, Hayat T, Alsaedi A. Numerical simulation of nanofluid forced convection heat transfer improvement in existence of magnetic field using lattice Boltzmann method. Int J Heat Mass Transf 2017; 108: 1870-1883.

[5] Wang X, He Y, Cheng G, Shi L, Liu X, Zhu J. Direct vapor generation through localized solar heating via carbon-nanotube nanofluid. Energy Convers Manage 2016; 130: 176-183.

[6] Shi L, He Y, Wang X, Hu Y. Recyclable photo-thermal conversion and purification systems via Fe_3O_4@TiO_2 nanoparticles. Energy Convers Manage 2018; 171: 272-278.

[7] Wang X, He Y, Liu X. Synchronous steam generation and photodegradation for clean water generation based on localized solar energy harvesting. Energy Convers Manage 2018; 173: 158-166.

[8] Liu X, Xuan Y. Full-spectrum volumetric solar thermal conversion via photonic nanofluids. Nanoscale 2017; 9(39): 14854-14860.

[9] Yu X, Xuan Y. Investigation on thermo-optical properties of CuO/Ag plasmonic nanofluids. Sol Energy 2018; 160: 200-207.

[10] Liu X, Wang X, Huang J, Cheng G, He Y. Volumetric solar steam generation enhanced by reduced graphene oxide nanofluid. Appl Energy 2018; 220: 302-312.

[11] Qi C, Hu J, Liu M, Guo L, Rao Z. Experimental study on thermo-hydraulic performances of CPU cooled by nanofluids. Energy Convers Manage 2017; 153:

557-565.

[12] Qi C, Zhao N, Cui X, Chen T, Hu J. Effects of half spherical bulges on heat transfer characteristics of CPU cooled by TiO_2-water nanofluids. Int J Heat Mass Transf 2018; 123: 320-330.

[13] Li H, Wang L, He Y, Hu Y, Zhu J, Jiang B. Experimental investigation of thermal conductivity and viscosity of ethylene glycol based ZnO nanofluids. Appl Therm Eng 2015; 88: 363-368.

[14] Ranjbarzadeh R, Moradikazerouni A, Bakhtiari R, Asadi A, Afrand M. An experimental study on stability and thermal conductivity of water/silica nanofluid: Eco-friendly production of nanoparticles. J Clean Prod 2019; 206: 1089-1100.

[15] Alnaqi AA, Aghakhani S, Pordanjani AH, Bakhtiari R, Asadi A, Tran MD. Effects of magnetic field on the convective heat transfer rate and entropy generation of a nanofluid in an inclined square cavity equipped with a conductor fin: Considering the radiation effect. Int J Heat Mass Transf 2019; 133: 256-267.

[16] Asadi A, Pourfattah F. Heat transfer performance of two oil-based nanofluids containing ZnO and MgO nanoparticles; a comparative experimental investigation. Powder Technol 2019; 343: 296-308.

[17] Asadi A, Asadi M, Rezaniakolaei A, Rosendahl LA, Afrand M, Wongwises S. Heat transfer efficiency of Al_2O_3-MWCNT/thermal oil hybrid nanofluid as a cooling fluid in thermal and energy management applications: An experimental and theoretical investigation. Int J Heat Mass Transf 2018; 117: 474-486.

[18] Asadi A, Asadi M, Rezaniakolaei M, Rosendahl LA, Wongwises S. An

experimental and theoretical investigation on heat transfer capability of $Mg(OH)_2$/MWCNT-engine oil hybrid nano-lubricant adopted as a coolant and lubricant fluid. Appl Therm Eng 2018; 129: 577-586.

[19] Asadi A, Asadi M, Rezaei M, Siahmargoi M, Asadi F. The effect of temperature and solid concentration on dynamic viscosity of MWCNT/MgO (20-80)-SAE50 hybrid nano-lubricant and proposing a new correlation: An experimental study. Int Commun Heat Mass Transf 2016; 78: 48-53.

[20] Esfe MH, Goodarzi M, Reiszadeh M, Afrand M. Evaluation of MWCNTs-ZnO/5W50 nanolubricant by design of an artificial neural network for predicting viscosity and its optimization. J Mol Liq 2019; 277: 921-931.

[21] Esfe MH, Reiszadeh M, Esfandeh S, Afrand M. Optimization of MWCNTs (10%)-Al_2O_3(90%)/5W50 nanofluid viscosity using experimental data and artificial neural network. Physica A 2018; 512: 731-744.

[22] Asadi M, Asadi A, Aberoumand S. An experimental and theoretical investigation on the effects of adding hybrid nanoparticles on heat transfer efficiency and pumping power of an oil-based nanofluid as a coolant fluid. Int J Refrig 2018; 89: 83-92.

[23] Asadi M, Asadi A. Dynamic viscosity of MWCNT/ZnO-engine oil hybrid nanofluid: an experimental investigation and new correlation in different temperatures and solid concentrations. Int Commun Heat Mass Transf 2016; 76: 41-45.

[24] Sheikholeslami M, Shamlooei M, Moradi R. Fe_3O_4-Ethylene glycol nanofluid

forced convection inside a porous enclosure in existence of Coulomb force. J Mol Liq 2018; 249: 429-437.

[25] Sheikholeslami M, Bhatti MM. Forced convection of nanofluid in presence of constant magnetic field considering shape effects of nanoparticles. Int J Heat Mass Transf 2017; 111:1039-1049.

[26] Afrand M, Toghraie D, Ruhani B. Effects of temperature and nanoparticles concentration on rheological behavior of Fe_3O_4-Ag/EG hybrid nanofluid: an experimental study. Exp Therm Fluid Sci 2016; 77: 38-44.

[27] Toghraie D, Alempour SM, Afrand M. Experimental determination of viscosity of water based magnetite nanofluid for application in heating and cooling systems. J Magn Magn Mater 2016; 417: 243-248.

[28] Afrand M. Experimental study on thermal conductivity of ethylene glycol containing hybrid nano-additives and development of a new correlation. Appl Therm Eng 2017; 110: 1111-1119.

[29] Qi C, Liu M, Luo T, Pan Y, Rao Z. Effects of twisted tape structures on thermo-hydraulic performances of nanofluids in a triangular tube. Int J Heat Mass Transf 2018; 127: 146-159.

[30] Hu Y, Li H, He Y, Wang L. Role of nanoparticles on boiling heat transfer performance of ethylene glycol aqueous solution based graphene nanosheets nanofluid. Int J Heat Mass Transf 2016; 96: 565-572.

[31] Qi C, Liang L, Rao Z. Study on the flow and heat transfer of liquid metal based nanofluid with different nanoparticle radiuses using two-phase lattice Boltzmann

method. Int J Heat Mass Transf 2016; 94: 316-326.

[32] Qi C, Wang G, Yang L, Wan Y, Rao Z. Two-phase lattice Boltzmann simulation of the effects of base fluid and nanoparticle size on natural convection heat transfer of nanofluid. Int J Heat Mass Transf 2017; 105: 664-672.

[33] Allouhi A, Amine MB, Saidur R, Kousksou T, Jamil A. Energy and exergy analyses of a parabolic trough collector operated with nanofluids for medium and high temperature applications. Energy Convers Manage 2018; 155: 201-217.

[34] Imani-Mofrad P, Heris SZ, Shanbedi M. Experimental investigation of the effect of different nanofluids on the thermal performance of a wet cooling tower using a new method for equalization of ambient conditions. Energy Convers Manage 2018; 158: 23-35.

[35] Loni R, Asli-Ardeh EA, Ghobadian B, Kasaeian A. Experimental study of carbon nano tube/oil nanofluid in dish concentrator using a cylindrical cavity receiver: Outdoor tests. Energy Convers Manage 2018; 165: 593-601.

[36] Asadi A. A guideline towards easing the decision-making process in selecting an effective nanofluid as a heat transfer fluid. Energy Convers Manage 2018; 175: 1-10.

[37] Rostami Z, Rahimi M, Azimi N. Using high-frequency ultrasound waves and nanofluid for increasing the efficiency and cooling performance of a PV module. Energy Convers Manage 2018; 160: 141-149.

[38] Bellos E, Tzivanidis C, Tsimpoukis D. Thermal, hydraulic and exergetic evaluation of a parabolic trough collector operating with thermal oil and molten

salt based nanofluids. Energy Convers Manage 2018; 156: 388-402.

[39] Sadeghinezhad E, Mehrali M, Rosen MA, Akhiani AR, Latibari ST, Mehrali M, Metselaar HSC. Experimental investigation of the effect of graphene nanofluids on heat pipe thermal performance. Appl Therm Eng 2016; 100: 775-787.

[40] Mehrali M, Sadeghinezhad E, Rosen MA, Akhiani AR, Latibari ST, Mehrali M, Metselaar HSC. Heat transfer and entropy generation for laminar forced convection flow of graphene nanoplatelets nanofluids in a horizontal tube. Int Commun Heat Mass Transf 2015; 66: 23-31.

[41] Mehrali M, Sadeghinezhad E, Rosen MA, Latibari ST, Mehrali M, Metselaar HSC, Kazi SN. Effect of specific surface area on convective heat transfer of graphene nanoplatelet aqueous nanofluids. Exp Therm Fluid Sci 2015; 68: 100-108.

[42] Mehrali M, Sadeghinezhad E, Rosen MA, Akhiani AR, Latibari ST, Mehrali M, Metselaar HSC. Experimental investigation of thermophysical properties, entropy generation and convective heat transfer for a nitrogen-doped graphene nanofluid in a laminar flow regime. Adv Powder Technol 2016; 27(2): 717-727.

[43] Sundar LS, Singh MK, Sousa AC. Heat transfer and friction factor of nanodiamond-nickel hybrid nanofluids flow in a tube with longitudinal strip inserts. Int J Heat Mass Transf 2018; 121: 390-401.

[44] Sundar LS, Bhramara P, Kumar NR, Singh MK, Sousa AC. Experimental heat transfer, friction factor and effectiveness analysis of Fe_3O_4 nanofluid flow in a horizontal plain tube with return bend and wire coil inserts. Int J Heat Mass

Transf 2017; 109: 440-453.

[45] Ranjbarzadeh R, Karimipour A, Afrand M, Isfahani AHM, Shirneshan A. Empirical analysis of heat transfer and friction factor of water/graphene oxide nanofluid flow in turbulent regime through an isothermal pipe. Appl Therm Eng 2017; 126: 538-547.

[46] Goodarzi M, Kherbeet AS, Afrand M, Sadeghinezhad E, Mehrali M, Zahedi P, Wongwises S, Dahari M. Investigation of heat transfer performance and friction factor of a counter-flow double-pipe heat exchanger using nitrogen-doped, graphene-based nanofluids. Int Commun Heat Mass Transf 2016; 76: 16-23.

[47] Ranjbarzadeh R, Isfahani AM, Afrand M, Karimipour A, Hojaji M. An experimental study on heat transfer and pressure drop of water/graphene oxide nanofluid in a copper tube under air cross-flow: applicable as a heat exchanger. Appl Therm Eng 2017; 125: 69-79.

[48] Shahsavani E, Afrand M, Kalbasi R. Using experimental data to estimate the heat transfer and pressure drop of non-Newtonian nanofluid flow through a circular tube: applicable for use in heat exchangers. Appl Therm Eng 2018; 129: 1573-1581.

[49] Xu H, Gong L, Huang S, Xu M. Flow and heat transfer characteristics of nanofluid flowing through metal foams. Int J Heat Mass Transf 2015; 83: 399-407.

[50] Sheikholeslami M, Jafaryar M, Li Z. Nanofluid turbulent convective flow in a circular duct with helical turbulators considering CuO nanoparticles. Int J Heat

Mass Transf 2018; 124: 980-989.
[51] Sheikholeslami M, Darzi M, Sadoughi MK. Heat transfer improvement and pressure drop during condensation of refrigerant-based nanofluid: an experimental procedure. Int J Heat Mass Transf 2018; 122: 643-650.
[52] Naphon P, Wiriyasart S. Pulsating TiO_2/water nanofluids flow and heat transfer in the spirally coiled tubes with different magnetic field directions. Int J Heat Mass Transf 2017; 115: 537-543.
[53] Naphon P, Wiriyasart S, Arisariyawong T, Nualboonrueng T. Magnetic field effect on the nanofluids convective heat transfer and pressure drop in the spirally coiled tubes. Int J Heat Mass Transf 2017; 110:739-745.
[54] Li Z, Sheikholeslami M, Jafaryar M, Shafee A, Chamkha AJ. Investigation of nanofluid entropy generation in a heat exchanger with helical twisted tapes. J Mol Liq 2018; 266: 797-805.
[55] Sheikholeslami M, Jafaryar M, Ganji DD, Li Z. Exergy loss analysis for nanofluid forced convection heat transfer in a pipe with modified turbulators. J Mol Liq 2018; 262: 104-110.
[56] Sheikholeslami M, Jafaryar M, Li Z. Second law analysis for nanofluid turbulent flow inside a circular duct in presence of twisted tape turbulators. J Mol Liq 2018; 263: 489-500.
[57] Qi C, Yang L, Chen T, Rao Z. Experimental study on thermo-hydraulic performance of TiO_2-H_2O nanofluids in a horizontal elliptical tube. Appl Therm Eng 2018; 129: 1315-1324.

[58] Zhai X, Qi C, Pan Y, Luo T, Liang L. Effects of screw pitches and rotation angles on flow and heat transfer characteristics of nanofluids in spiral tubes. Int J Heat Mass Transf 2019; 130: 989-1003.

[59] Mei S, Qi C, Luo T, Zhai X, Yan Y. Effects of magnetic field on thermo-hydraulic performance of Fe_3O_4-water nanofluids in a corrugated tube. Int J Heat Mass Transf 2019; 128: 24-45.

[60] Karimi A, Afrand M. Numerical study on thermal performance of an air-cooled heat exchanger: Effects of hybrid nanofluid, pipe arrangement and cross section. Energy Convers Manage 2018; 164: 615-628.

[61] Bahiraei M, Salmi HK, Safaei MR. Effect of employing a new biological nanofluid containing functionalized graphene nanoplatelets on thermal and hydraulic characteristics of a spiral heat exchanger. Energy Convers Manage 2019; 180: 72-82.

[62] Sharshir SW, Peng GL, Elsheikh AH, Edreis EMA, Eltawil MA, Abdelhamid T, Kabeel AE, Zang JF, Yang N. Energy and exergy analysis of solar stills with micro/nano particles: A comparative study. Energy Convers Manage 2018; 177: 363-375.

[63] Bahiraei M, Heshmatian S. Thermal performance and second law characteristics of two new microchannel heat sinks operated with hybrid nanofluid containing grapheme-silver nanoparticles. Energy Convers Manage 2018; 168: 357-370.

[64] Qiu L, Deng HW, Sun JN. Pressure drop and heat transfer in rotating smooth square U-duct under high rotation numbers. Heat Mass Transfer 2013; 66:

543-552.

[65] Qi C, Wang G, Yan Y, Mei S, Luo T. Effect of rotating twisted tape on thermo-hydraulic performance of nanofluids in heat-exchanger systems. Energy Convers Manage 2018; 166: 744-757.

[66] Qi C, Wan YL, Li CY, Han DT, Rao ZH. Experimental and numerical research on the flow and heat transfer characteristics of TiO_2-water nanofluids in a corrugated tube. Int J Heat Mass Transf 2017; 115: 1072-1084.

[67] Pak BC, Cho YI. Hydrodynamic and heat transfer study of dispersed fluids with submicron metallic oxide particles. Exp Heat Transfer 1998; 11(2): 151-170.

[68] Yang SM, Tao WQ. Heat Transfer, 4th ed. Beijing: Higher Education Press; 2012.